

Optically Pumped NMR Studies of Electron Spin Polarization and Dynamics: New Constraints on the Composite Fermion Description of $\nu = 1/2$

A. E. Dementyev¹, N. N. Kuzma¹, P. Khandelwal¹, S. E. Barrett¹, L. N. Pfeiffer², and K. W. West²

¹*Department of Physics, Yale University, New Haven, Connecticut 06511*

²*Bell Laboratories, Lucent Technologies, Murray Hill, New Jersey 07974*

(September 4, 2018)

The Knight shift and the nuclear spin-lattice relaxation rate $1/T_1$ of ^{71}Ga nuclei are measured in GaAs quantum wells at Landau level filling factor $\nu = 1/2$ using optically pumped NMR. The temperature dependences of these data are compared with predictions of a weakly-interacting composite fermion model. Our measurements of the electron spin polarization and spin dynamics near the transition between fully and partially spin-polarized ground states provide new constraints on the theoretical description of $\nu = 1/2$.

Significant progress in describing a strongly interacting 2-dimensional electron system (2DES) in a large magnetic field in terms of composite fermions (CF) in a reduced field has stimulated a large body of theoretical and experimental work [1,2]. One of the most surprising implementations of this idea was put forth in the seminal work of Halperin, Lee, and Read [3], who argued that the ground state of the 2DES at Landau level filling factor $\nu = \frac{1}{2}$ is well-described by CF in zero net magnetic field, which therefore exhibit a well-defined Fermi surface. Experiments carried out near $\nu = \frac{1}{2}$ have provided convincing evidence of the existence of the CF Fermi surface [4,5,6,7,8].

Despite the overall agreement between theory and experiment to date, several fundamental issues about CF at $\nu = \frac{1}{2}$ have yet to be resolved experimentally. For example, do CF form a Fermi gas, a “normal” Fermi liquid, or some kind of “unusual” Fermi liquid? Also, does the picture change when the ground state is only partially spin-polarized [9,10,11]? Experiments which directly probe the electron spin degree of freedom *right at* $\nu = \frac{1}{2}$, especially near the transition between partially and fully spin-polarized ground states, will help to answer these central questions.

In this Letter, we report optically pumped nuclear magnetic resonance (OPNMR) [12] measurements of the Knight Shift K_S and the spin-lattice relaxation rate $1/T_1$ of ^{71}Ga nuclei in two different electron-doped multiple quantum well (MQW) samples. The K_S data reveal the spin polarization $\mathcal{P}(T) \equiv \frac{\langle S_z(T) \rangle}{\max\langle S_z \rangle}$, while the $1/T_1$ data probe the spin dynamics of the 2DES. Taken together, these thermodynamic measurements provide unique insights into the physics of CF at $\nu = \frac{1}{2}$.

The two samples used in this work were previously studied [13,14] near $\nu = \frac{1}{3}$. Sample 40W contains forty 300 Å wide GaAs wells separated by 3600 Å wide $\text{Al}_{0.1}\text{Ga}_{0.9}\text{As}$ barriers. Sample 10W contains ten 260 Å wide wells separated by 3120 Å wide barriers. Silicon delta-doping spikes located in the center of each barrier provide the electrons that are confined in each GaAs well

at low temperatures, producing 2DES with very high mobility ($\mu > 1.4 \times 10^6 \text{ cm}^2/\text{Vs}$). This MQW structure results in a 2D electron density that is unusually insensitive to light, and extremely uniform from well to well [15]. The low temperature ($0.29 < T < 3.5 \text{ K}$) OPNMR measurements described below were performed using a sorption-pumped ^3He cryostat. The samples, about $4 \times 6 \text{ mm}^2$ in size, were in direct contact with ^3He , mounted on the platform of a rotator assembly in the NMR probe. Data were acquired following the previously described [13,14,16,17] OPNMR timing sequence: SAT- τ_L - τ_D -DET, modified for use below 1 Kelvin (e.g., $\tau_D > 10 \text{ s}$, laser power $\sim 10 \text{ mW/cm}^2$, low rf voltage levels). A calibrated RuO_2 sensor, in good thermal contact with the sample, was used to monitor the temperature. The peak in $K_S(\nu)$ at $\nu=1$ was used to determine the electron density n for each sample [13]. Using the rotator assembly, we could set the angle θ between the sample’s growth axis and the applied field B_{tot} so that the filling factor $\nu = nhc/eB_{\perp}$ (with $B_{\perp} \equiv B_{\text{tot}} \cos \theta$) equalled $\frac{1}{2}$ for these three cases:

Case	Sample	B_{tot} [T]	θ	n [cm^{-2}]	w [Å]
I	40W	7.03	38.3°	6.69×10^{10}	300
II	40W	5.52	0.0°	6.69×10^{10}	300
III	10W	7.03	24.5°	7.75×10^{10}	260

Figure 1 shows OPNMR spectra at $\nu = \frac{1}{2}$ and $T \approx 0.5 \text{ K}$, for Cases I–III (a-c, solid lines). Nuclei within the quantum wells are coupled to the spins of the 2DES via the isotropic Fermi contact interaction [18], which shifts the corresponding well resonance (labeled “W” on Fig. 1(c)) relative to the signal from the barriers (“B”) [16,17]. We define the Knight shift K_S as the peak-to-peak splitting between “W” and “B”. For Case I, all spectra (e.g., Fig. 1(a)) are well-described by the same two-parameter fit (dotted lines) [13,14] that was used for all spectra at $\nu = \frac{1}{3}$. This fit is generated under the assumption that all spins are delocalized, so that $\langle S_z(\nu, T) \rangle$, averaged over the NMR time scale ($\sim 40 \mu\text{sec}$), appears spatially homogeneous along the plane of the wells, and thus the resulting lineshape is “motionally-narrowed” [18].

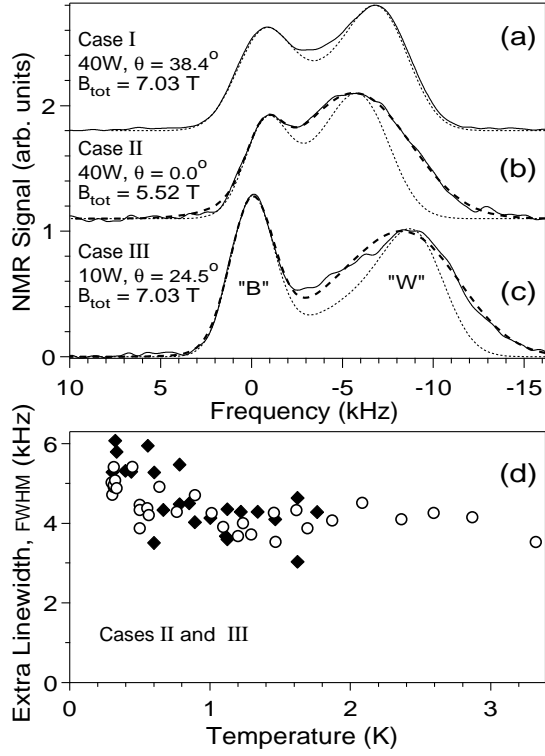


FIG. 1. ^{71}Ga OPNMR spectra (a-c, solid lines) at $\nu=\frac{1}{2}$, $T \approx 0.5\text{ K}$. The dotted line fits (a-c) use a 3.5 KHz FWHM Gaussian broadening (due to nuclear spin-spin coupling) of the intrinsic well and barrier lines. The dashed line fits (b,c) require an extra Gaussian broadening of “W” with the FWHM shown in (d) for samples 40W (open circles) and 10W (filled diamonds).

In contrast, for Cases II and III, the well resonance (Fig. 1(b,c)) is much broader than the same fit (dotted lines). An additional gaussian broadening of just the well resonance leads to a better fit (dashed lines). The full width at half maximum (FWHM) of the additional broadening extracted from these fits is plotted in Fig. 1(d) for Cases II and III. Earlier measurements at $\nu < \frac{1}{3}$ and $T \approx 0.5\text{ K}$ were also poorly described by the “motionally-narrowed” lineshape, but in that case the extra well width was sharply temperature-dependent [14], whereas here it is essentially independent of temperature. The extra broadening of the well lineshape for Cases II and III (Fig. 1(b,c,d)) seems to be homogeneous [19], if so, the corresponding transverse relaxation time T_2 [18] is quite short. The origin of this effect is not understood as it is very hard to explain simultaneously the temperature-independence of the extra broadening and the lack of a similar effect in Case I.

Figure 2(a) shows $K_S(T)$ at $\nu=\frac{1}{2}$ for Cases I–III. The larger scatter in the $K_S(T)$ data for Cases II and III is a consequence of the large linewidth. Using an empirical relation (all in kHz) $K_{S\text{int}} = K_S + 1.1 \times (1 - \exp(-K_S/2.0))$, we can convert K_S into

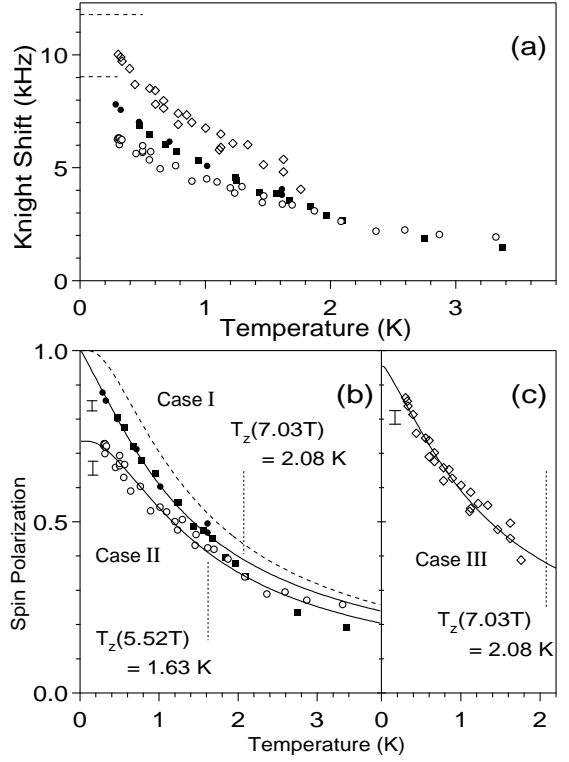


FIG. 2. Temperature dependence at $\nu=\frac{1}{2}$ of (a) K_S and (b, c) \mathcal{P} for Case I (open diamonds), Case II (filled symbols), and Case III (open circles). Note the error bars in (b,c). The solid and dashed curves are described in the text.

$K_{S\text{int}}$, which is the intrinsic hyperfine shift for the nuclei in the center of each well. $K_{S\text{int}} = A_c \mathcal{P} n/w$ is a direct measure of the electron spin polarization \mathcal{P} , where w is the width of each well and $A_c = (4.5 \pm 0.2) \times 10^{-13}\text{ cm}^3/\text{s}$ is the hyperfine constant [13]. For Cases II and III, the same values of $K_{S\text{int}}(T)$ are also obtained directly from the dashed line fits (e.g., Fig. 1(b,c)).

$K_{S\text{int}}(T)$ is converted to electron spin polarization using $\mathcal{P}(\nu=\frac{1}{2}, T) = K_{S\text{int}}(T)/K_{S\text{int}}^{\mathcal{P}=1}$, where the maximum shift for a fully polarized 2DES is known for each sample: $K_{S\text{int}}^{\mathcal{P}=1} = K_{S\text{int}}(\nu=\frac{1}{3}, T \rightarrow 0)$ [13].

Figure 2(b,c) shows that $\mathcal{P}(\nu=\frac{1}{2}, T)$ does not saturate down to our base temperature of 0.29 K, in contrast to earlier measurements at $\nu=1$ and $\frac{1}{3}$ [13,16]. Moreover, as the temperature is increased, $\mathcal{P}(\nu, T)$ falls off much faster at $\nu=\frac{1}{2}$ than at $\nu=1$ or $\frac{1}{3}$ (e.g., at $T_Z = |g^* \mu_e B_{\text{tot}}/k_B|$, $\mathcal{P}(\nu=1, T_Z) \approx 93\%$, while $\mathcal{P}(\nu=\frac{1}{2}, T_Z) \approx 40\%$. Here $g^* = -0.44$, μ_e is the Bohr magneton and k_B is the Boltzmann constant). Qualitatively, these results are consistent with a tiny (or vanishing) energy gap for spin-flip excitations at $\nu=\frac{1}{2}$ for Cases I–III. However, a quantitative understanding of the $\mathcal{P}(\nu=\frac{1}{2}, T)$ data remains a challenge for theory (e.g., we cannot explain the crossing of the Case I and Case II data sets at $T \approx T_Z$ (Fig. 2(b))).

Even though saturation is not observed, the Knight

shift data for Case II are evidence for a $\nu=\frac{1}{2}$ ground state in which the electrons are only *partially* spin-polarized (i.e., $\mathcal{P}(\nu=\frac{1}{2}, T \rightarrow 0) \approx 70 - 85\%$). This inference is consistent with data obtained from two other experiments in conditions similar to those of Case II. From their time-resolved photoluminescence measurements, Kukushkin et al. [10] estimate $\mathcal{P}(\nu=\frac{1}{2}, T \rightarrow 0) \approx 87\%$ at 5.52 T. Surface acoustic wave measurements of Willett et al. obtained a Fermi wave vector which was $\sim 90\%$ of the theoretical value for fully polarized CF, consistent with a polarization of at least $\mathcal{P}(\nu=\frac{1}{2}, T \rightarrow 0) \approx 62\%$. [4]

The solid curves in Figure 2(b,c) are two parameter fits to the $T < T_Z$ data using expressions for $\mathcal{P}(\nu=\frac{1}{2}, T)$ derived within a weakly-interacting composite fermion model (WICFM). In this model, the dispersion relations for spin-up and spin-down states are:

$$E_{\uparrow}(k) = \frac{\hbar^2 k^2}{2m^*}, \quad E_{\downarrow}(k) = \frac{\hbar^2 k^2}{2m^*} + E_Z^*(T), \quad (1)$$

where an exchange interaction has been included in the model through the effective Zeeman energy:

$$E_Z^*(T) = |g^* \mu_e B_{\text{tot}}| + E_{\text{Exch}} = k_B T_Z + k_B J \mathcal{P}(T). \quad (2)$$

When $J = 0$, this is just the non-interacting composite fermion model [10]. When $J > 0$, there is a Stoner enhancement of the spin susceptibility. In this model, the chemical potential μ and the polarization \mathcal{P} are:

$$\mu(T) = k_B T \ln \left(-\gamma + \sqrt{\gamma^2 + \exp(\rho) - 1} \right) + \frac{E_Z^*(T)}{2} \quad (3)$$

$$\mathcal{P}(T) = \frac{1}{\rho} \ln \left(\frac{1 + \exp[\frac{\mu(T)}{k_B T}]}{1 + \exp[\frac{\mu(T)}{k_B T} (1 - \delta(T))]} \right) \quad (4)$$

where $\gamma = \cosh(\frac{E_Z^*(T)}{2k_B T})$; $\rho = \frac{2\pi\hbar^2 n}{m^* k_B T}$; and $\delta(T) = \frac{E_Z^*(T)}{\mu(T)}$.

Equations 2–4 are solved self-consistently for $\mathcal{P}(T)$ at each m^* and J . Within this WICFM, the behavior of $\mathcal{P}(T)$ as $T \rightarrow 0$ is quite sensitive to the parameter $\delta(0)$. The ground state is only fully polarized ($\mathcal{P}(0)=1$) when $\delta(0) \geq 1$. We find $\delta(0) < 1$ for Cases II and III, $\delta(0)=1$ for Case I, and the dashed curve illustrates $\delta(0) > 1$ (Fig. 2(b,c)). Thus, within this model, the best-fit curves for Cases II and III yield partially-polarized ground states, while Case I is fully-polarized. As described earlier, Cases II and III also have extra linewidth, while Case I does not (Fig. 1).

Figure 3 shows the temperature dependence of the ^{71}Ga nuclear spin-lattice relaxation rate $1/T_1$ at $\nu=\frac{1}{2}$ for Cases I and II. At each temperature, OPNMR spectra were acquired using a series of dark times $10\text{ s} \leq \tau_D \leq 2560\text{ s}$ (i.e., the longest $\tau_D \geq 4T_1$). The value of $1/T_1$ was determined by fitting the signal intensity at the “W” peak frequency to the form $S(\tau_D) =$

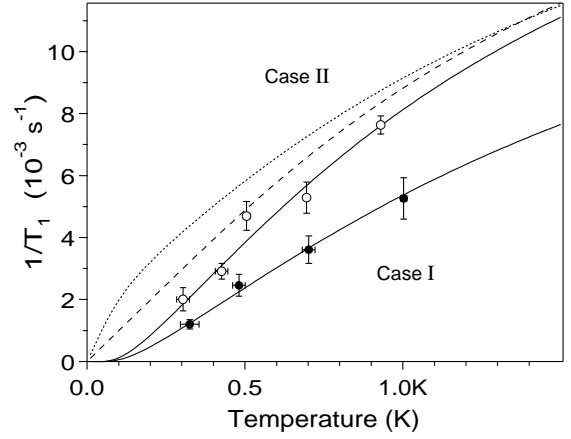


FIG. 3. Temperature dependence of the ^{71}Ga spin-lattice relaxation rate $1/T_1$ at $\nu=\frac{1}{2}$ for Case I (filled symbols) and Case II (open symbols). The solid and dashed curves are described in the text.

$S_0 \exp(-\tau_D/T_1) + S_1$. Note that these $T < T_Z$ relaxation rates are faster than the rate at $T \approx T_Z$ for $\nu=1$ [17]. Qualitatively, this shows that there is a greater overlap of the density of states for electrons with opposite spins at $\nu=\frac{1}{2}$ than at $\nu=1$.

The isotropic Fermi contact hyperfine coupling between the electron spins and the nuclear spins is responsible for both K_S and $1/T_1$ [13,14,16,17], as is the case for some metals [18,20]. Within the WICFM, $1/T_1(\nu=\frac{1}{2}, T)$ for ^{71}Ga nuclei in the center of the quantum well is:

$$\frac{1}{T_1} = \frac{\pi(m^*)^2}{\hbar^3} \left(\frac{K_{\text{Sint}}^{\mathcal{P}=1}}{n} \right)^2 \frac{k_B T}{1 + \exp[\frac{\mu(T)}{k_B T} (\delta(T) - 1)]}. \quad (5)$$

This expression is used as a two-parameter fit to the $1/T_1(T)$ data (Fig. 3, solid lines), where $\mu(T)$ and $\delta(T)$ are obtained from Eqns. 2–4 for each m^* and J . The behavior of $1/T_1(T)$ as $T \rightarrow 0$ is also quite sensitive to the parameter $\delta(0)$. In Fig. 3, we illustrate $\delta(0) < 1$ with the dotted curve, $\delta(0)=1$ with the dashed curve, and we find $\delta(0) > 1$ for Cases I and II (solid curves). In contrast to normal metals, here $\mu(0) \sim |g^* \mu_e B_{\text{tot}}|$.

Figure 4 shows the best values of J and m^* obtained for each data set in Figs. 2(b,c) and 3. The correlation between J and m^* is shown by $\Delta\chi^2=1$ and $\Delta\chi^2=4$ contours. These (J, m^*) values lie quite close to the curves which mark the transition between fully and partially polarized ground states (i.e., where $\delta(0)=1$). There is negligible overlap between the contours and the line $J=0$, so the non-interacting composite fermion model used by Kukushkin et al. [10] does not work here. Moreover, there is no (J, m^*) pair which can simultaneously describe the four data sets measured using the same sample and B_{\perp} (Fig. 4 (main)), so we conclude that even the weakly-interacting composite fermion model is a poor description of the $\nu=\frac{1}{2}$ state for these Cases. The most glaring inconsistency is that of Case II, where $\delta(0) < 1$ (i.e.,

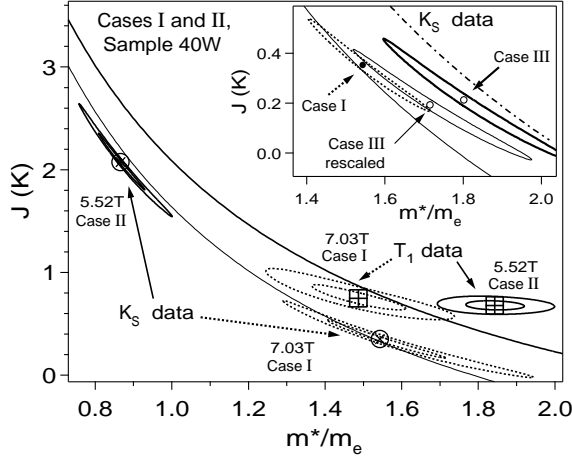


FIG. 4. Values of J (in Kelvin) and m^* (in units of the electron mass in vacuum, m_e), obtained using a χ^2 analysis of : (main) $\mathcal{P}(T)$ (circles) and $1/T_1(T)$ (squares) for Case I (dashed contours) and Case II (solid contours), and (inset) $\mathcal{P}(T)$ for Case I (dashed contour) and Case III (thick solid contour). The thin solid contour in the inset shows the rescaled Case III values described in the text. Within the WICFM, the ground state is fully spin-polarized for (J, m^*) values that lie above the thin solid curve (Case I), thick solid curve (Case II), or dashed-dotted curve (Case III, inset).

partially-spin polarized at $T=0$) is inferred from $\mathcal{P}(T)$, which is *incompatible* with the result $\delta(0) > 1$ (i.e., fully-spin polarized at $T=0$) that is inferred from $1/T_1(T)$.

Figure 4 (inset) shows the (J, m^*) values obtained from the $\mathcal{P}(T)$ data for Cases I and III. These values do not agree, however, sample 10W and 40W also have slightly different electron densities and well widths (n, w). This would affect our results, since we expect $k_B J \propto eB_{\perp}/m^* \propto E_C(\lambda) \equiv e^2/(\epsilon\sqrt{l_0^2 + \lambda^2})$, where $l_0 = \sqrt{\hbar c/eB_{\perp}}$ is the magnetic length, $\epsilon=13$, and the parameter $\lambda \approx \frac{1}{4}w$ modifies the Coulomb energy scale due to the non-zero thickness w of the quantum well [21]. To correct for this, the Case III (J, m^*) values are rescaled using:

$$\frac{J(n_I, w_I)}{J(n_{III}, w_{III})} = \sqrt{\frac{n_I}{n_{III}} \left(\frac{1 + \frac{n_I w_I^2}{n_{III} w_{III}^2}}{2} \right)},$$

$$\frac{m^*(n_I, w_I)}{m^*(n_{III}, w_{III})} = \sqrt{\frac{n_I}{n_{III}} \left(\frac{2}{1 + \frac{n_I w_I^2}{n_{III} w_{III}^2}} \right)}. \quad (6)$$

The rescaled contour has a good overlap with the (J, m^*) values for Case I (Fig. 4 (inset)). This rescaling is irrelevant for Fig. 4 (main), where the results on a single sample are shown.

In conclusion, neither a non-interacting nor a weakly-interacting composite fermion model is sufficient to explain our experiments, which probe the electron spin degree of freedom *right at* $\nu = \frac{1}{2}$. Knight shift and $1/T_1$ data, taken together, provide important new con-

straints on the theoretical description of the $\nu = \frac{1}{2}$ state. Finally, in addition to fully polarized ground states (Case I, $\frac{k_B T_Z}{E_C(\lambda)} = 0.021$), partially spin-polarized ground states (Cases II and III, $\frac{k_B T_Z}{E_C(\lambda)} = 0.017$ and 0.019) are experimentally accessible, and exhibit unexpected features (e.g., the extra linewidth).

We thank N. Read, R. Shankar, S. Sachdev, and R. L. Willett for many helpful discussions. This work was supported by NSF Grant #DMR-9807184. SEB also acknowledges an Alfred P. Sloan Research Fellowship.

-
- [1] For comprehensive reviews, see: *Composite Fermions*, ed. by O. Heinonen (World Scientific, 1998); *Perspectives in Quantum Hall Effects*, ed. by S. Das Sarma and A. Pinczuk (Wiley, New York, 1997); J. K. Jain, *Adv. Phys.* **41**, 105 (1992); R. L. Willett, *ibid.* **46**, 447 (1997).
 - [2] For recent theoretical developments near $\nu = \frac{1}{2}$, see: N. Read, *Phys. Rev. B* **58**, 16262 (1998); A. Stern, B. I. Halperin, F. v. Oppen, and S. H. Simon, *ibid.* **59**, 12547 (1999); R. Shankar, cond-mat/9903064.
 - [3] B. I. Halperin, P. A. Lee, and N. Read, *Phys. Rev. B* **47**, 7312 (1993).
 - [4] R. L. Willett, R. R. Ruel, K. W. West, and L. N. Pfeiffer, *Phys. Rev. Lett.* **71**, 3846 (1993).
 - [5] R. L. Willett, K. W. West, and L. N. Pfeiffer, *Phys. Rev. Lett.* **75**, 2988 (1995).
 - [6] W. Kang *et al.*, *Phys. Rev. Lett.* **71**, 3850 (1993).
 - [7] V. J. Goldman, B. Su, and J. K. Jain, *Phys. Rev. Lett.* **72**, 2065 (1994).
 - [8] J. H. Smet *et al.*, *Phys. Rev. Lett.* **77**, 2272 (1996).
 - [9] R. R. Du *et al.*, *Phys. Rev. Lett.* **75**, 3926 (1995).
 - [10] I. V. Kukushkin, K. v. Klitzing, and K. Eberl, *Phys. Rev. Lett.* **82**, 3665 (1999).
 - [11] K. Park and J. K. Jain, *Phys. Rev. Lett.* **80**, 4237 (1998).
 - [12] S. E. Barrett, R. Tycko, L. N. Pfeiffer, and K. W. West, *Phys. Rev. Lett.* **72**, 1368 (1994).
 - [13] P. Khandelwal *et al.*, *Phys. Rev. Lett.* **81**, 673 (1998); also available at cond-mat/9801199.
 - [14] N. N. Kuzma *et al.*, *Science* **281**, 686 (1998); also available at cond-mat/9907279.
 - [15] L. N. Pfeiffer *et al.*, *Appl. Phys. Lett.* **61**, 1211 (1992).
 - [16] S. E. Barrett *et al.*, *Phys. Rev. Lett.* **74**, 5112 (1995).
 - [17] R. Tycko *et al.*, *Science* **268**, 1460 (1995).
 - [18] C. P. Slichter, *Principles of Magnetic Resonance* (Springer, New York, 1990), 3rd ed.
 - [19] In simulations, we found that an unreasonably large FWHM of 70% or more is required for a gaussian distribution of electron densities along the well to explain the large temperature independent linewidth observed at $\nu = \frac{1}{2}$ for Cases II and III.
 - [20] J. Winter, *Magnetic Resonance in Metals*, (Oxford Univ. Press, London, 1971).
 - [21] F. C. Zhang and S. Das Sarma, *Phys. Rev. B* **33**, 2903 (1986).